Chapter 4. Photocatalytic and Lithium Ion Intercalation Properties of Titanate Nanostructures Produced by Solvothermal Method

4.1. Introduction

4.1.1. Photoactive titanate nanostructure

The photocatalysis phenomena, which occur on the surface of semiconductor by photoinduced electron-hole pair and reactant, are generally acknowledged. The majority of scientists accepted that there are two most important points to improve photocatalytic efficiency. One is modifying the structure of materials to enhance the yield of photoinduced electron-hole pair; another is to increase surface area of materials.[1] However, the first one is more critical. If the photoactivity is not high, the efficiency can not be improved effectively by increasing the surface area.

To increase surface area, the most direct route is to decrease the size of our material. Therefore, the titanium oxide nanostructures obtained much attention in the photoinduced applications. Recently, the titanate nanotube which has large specific surface became a hot subject in photocatalysis.[2-8] However, the nanotube without doping with other atom, metal or semiconductor is inactive. As for other structures as nanosheet and nanowire, they have rarely been studied. Recently, V. Štengl et al. reported the photoactivity of $Na_2Ti_6O_{13}$ phase semi-tubular titanate product obtained by annealing semi-tubular sodium hydroxo titanate to over 550° C.[9] But, the efficiency is not better than Degussa P25 TiO_2. In this chapter, we tested the photocatalytic property of various titania nanostructures obtained from ion exchanged and annealed sodium hydroxo titanate samples. We found the nanosheet and nanowire are photoactive but not nanotube. We try to explain their different photoactivity by their unique preferred orientation and surface environment.

4.2.2. Lithium intercalated ability of titanate structure

Titanium oxide has been found to be a good candidate as lithium-ion host materials, due to its high capacity with low cost and non toxicity. In 1995, Huang et al. reported a capacity of 50 mAh/g for nanosized TiO_2.[10] In 2003, Zhou et al. used anatase form titanate nanotube produced by hydrothermal method to intercalate lithium. They reported bigger capacity as175 mAh/g and high reversibility.[11] In 2005, M. Zukalová et al. reported lithium ion intercalation property on TiO_2(B) fibers with high capacity and lower working potential (1.5V and 1.6V) than anatase.[12] This observation provides a possible non-aqueous supercapacitor material. A. R. Armstrong et al. reported that TiO_2(B) nanowire produced by hydrothermal method has a higher capacity than bulk one form conventional solid-state synthesis.[13]

In this study, we compare the lithium ion intercalation property of various titanate nanostructures involving nanosheet (anatase), nanotube (anatase) and nanowire (TiO_2(B)). For further study, we also compared nanofiber (small nanowire), carbonate additive nanowire and nanowire to discuss the size and carbonate effect of lithium ion intercalation.

4.2. Method

4.2.1. Photocatalyse (collaboration with Dr Eric Puzenat, LACE, UMR 5634, Université Claude Bernard Lyon1)

A. Materials

Malic acid (HOOC-CH_2-CHOH-COOH) was purchased from Aldrich with the highest purity grade (>99%).

B. Laboratory photoreactor and light source

The batch photoreactor was a cylindrical flask made of Pyrex of ca. 100mL with a bottom optical window of ca. 4 cm diameter and was open to air. Irradiation was provided by a high pressure mercury lamp (Philips HPK 125W) and was filtered by a circulating-water cell (thickness 2.2 cm) equipped with a 290 nm cut-off filter made of Pyrex. The water cell was used to remove IR radiation, thus preventing any heating of the suspension.

The radiant flux was measured with a radiometer detector from United Detector Technology company. The bandwidth of the radiometer was from 290 nm to 800nm. The total radiant flux was 40 $mW \cdot cm^{-2}$.

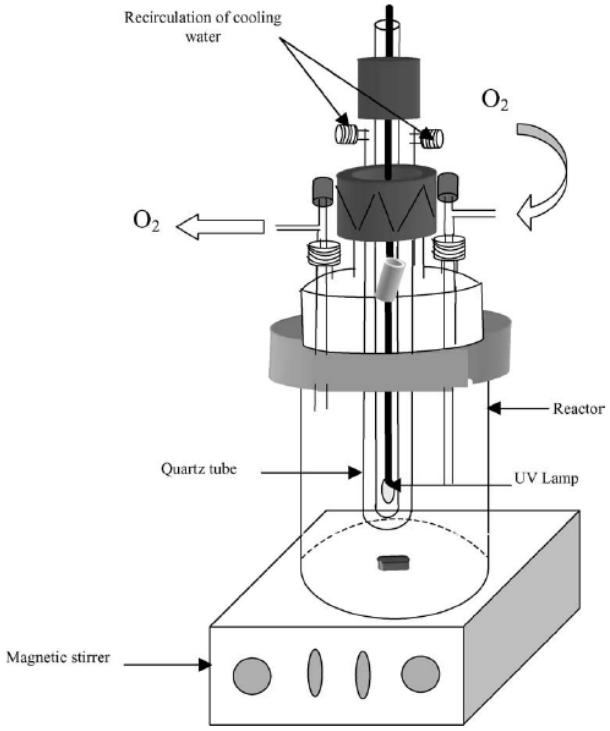

Figure 4.1. Photoreacter of photocatalysis.[14]

C. Photodegradation

The photocatalytic test was performed at room temperature (20°C). 30 mg TiO_2 were added, under stirring, to 30 mL of a 50 ppm (379 μmol L^{-1}) solution of malic acid and maintained in the dark for 30 min to reach to reach the adsorption equilibrium. At time t=0,

the photoreactor was irradiated. Samples from the suspension (0.5 mL) were taken at regular time intervals for analysis.

D. Analyses

Samples taken after different irradiation times, were filtered through 0.45 mm filters (Milipore) to remove TiO_2 particles before analysis.

The HPLC-UV analyses were performed using a VARIAN Prostar system with a polychrome detector adjusted at 210 nm and on a Car-H SARASEP column. The mobile phase was composed of H_2SO_4, $5x10^{-3}$ mol/l and the flow rate was 0.2ml/l.

4.2.2. Lithium ion intercalation (collaboration with Pr René Marchand and PrThierry Brousse, LGMA, Polytech, Nantes)

A. Materials

Bulk TiO_2(B) (as reference) The synthesis of our pristine titanate was performed according to the method developped by one of the authors (Marchand et al [19]) in 1982. Briefly, the starting material $K_2Ti_4O_9$ is obtained by heating KNO_3 (Merck, purity) and TiO_2 (anatase, Prolabo purity) in the molar ratio 1:2 at 1000°C for 6 hours. The resulting solid is ground in agate mortar and then hydrolysed for 3 days in HNO_3 < 0.5M (10^{-3} mol $K_2Ti_4O_9$ in 100 cm^3 HNO_3). After filtering, the powder was heated at 500°C in air for 15 hours.

Activated carbon Activated carbon was PICACTIF obtained from PICA Company. The resistivity was 1.99 Ω.cm.

B. Electrodes preparation

The TiO_2 (B) powder was mixed with acetylene black and Poly (vinylydene fluoride), PVDF, dissolved in n-methyl pyrolidinone, NMP, 6 wt %, in a weight ratio 71.5 :22.5 :6.0. The slurry was mixed overnight to obtain an homogeneous black paste which is then barcoated on a copper foil and the solvent is removed at 100°C in air for 2 hours. Pieces 14 mm diameter were then cut and used as the electrode in homemade cells assembled inside an argon filled glove box. The average amount of TiO_2 (B) in a round piece of electrode is about 2.5 mg. Each electrode was carefully weighted before use and several electrodes were tested to assume the reproducibility of the electrochemical behavior.

Activated carbon electrodes were prepared by laminating dried active material onto 4 cm^2 Aluminium current collector. Current collector is a treated-Al grid collector (100 µm thick) covered by a conductive paint. Composition of the active material is 95% of activated carbon PICACTIF and 5% of Polytetrafluoroethylene as binder (PTFE).

C. Electrochemical tests

The samples were tested with a Mac-Pile equipment (BioLogic), using a two-electrodes cell and metallic lithium as the counter electrode. The electrolyte used was 1 M solution of $LiPF_6$ in ethylene carbonate: diethyl carbonate (Merck), with a molar ratio of 1:2. Glass fiber paper was used as separator. Alternatively, an Arbin BT2000 battery tester was used to perform the 3-electrode measurements, with TiO_2(B) as the negative (working electrode), PICACTIF as the positive (counter electrode) and lithium as the reference electrode.

4.3. Results and Discussions

4.3.1. Photocatalytic property of titanate nanotructures

In the first series of samples (figure 4.2), we examined the proton exchanged and annealed nanotube and nanosheet, respectively. We found that annealed samples with anatase phase are much more photoactive than only proton exchanged ones. The annealed exchanged nanosheet has similar efficiency with Degussa P25 TiO_2, but worse adsorption ability. Therefore the P25 completed the reaction earlier. In fact, due to the excellent adsorbability with reactant, P25 has degenerated 40% of reactant in the beginning of experiment. The difference of adsorption property between nanosheet and P25 may be due to the intercalated carbonate which occupies some of the active sites. These adsorbed carbonates have been discussed many times in the previous chapters. We can obviously observe their existence in FT-IR, Ramanand TGA-MS results. These adsorbed carbonate can be eliminated after the first irradiation. Although the nanotube has very big specific surface, its photocatalytic efficiency is worse than annealed nanosheet and P25. That may be because the curvature and distortion of nanotube structure induces many defaults during proton exchanging and calcinations. In nanosheet case, the titanate layer is more planar; let it be able to shift to reconstruct the H-form structure, so that less defaults may occurr. We acknowledged that the defaults of TiO_2 crystal often reduce the efficiency of photocatalysis.

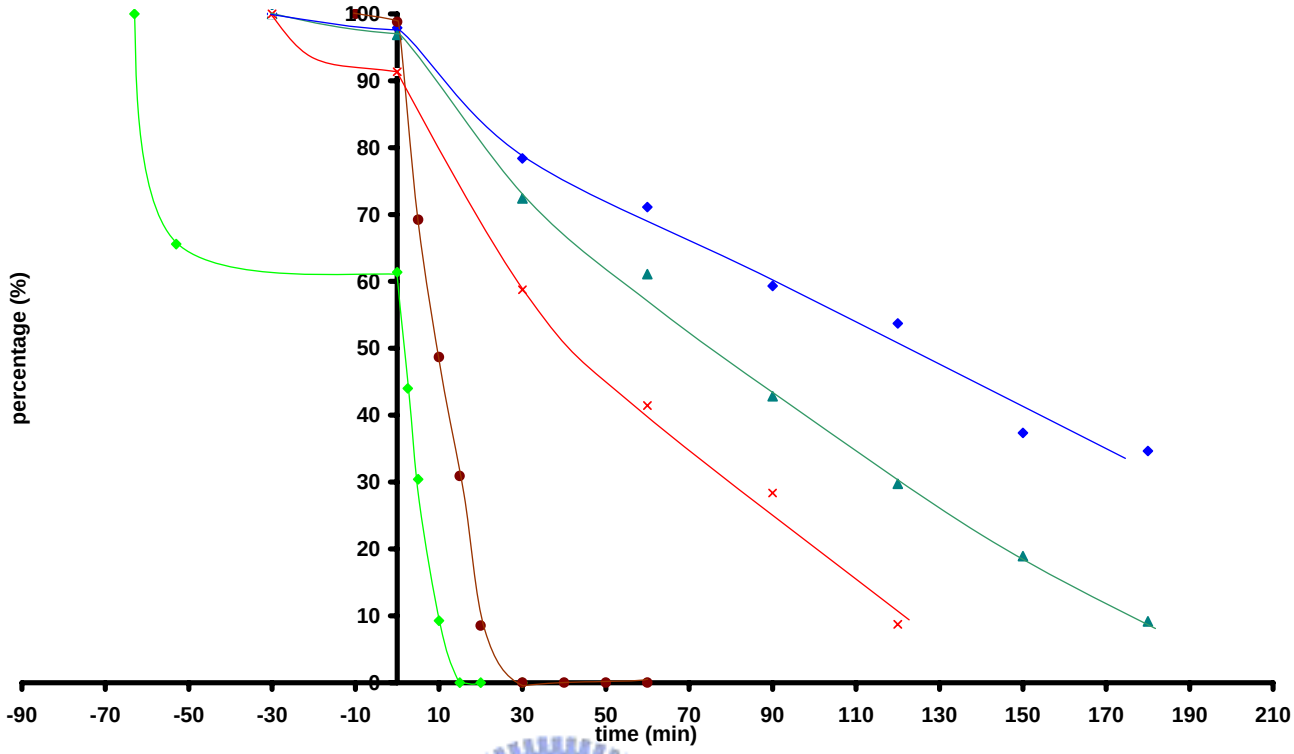

Figure 4.2. Photocatalytic activity of ▲: H-nanotube (RDH10MR-H), x: annealed H-nanotube (RDH10MR-H-400˚ C), ♦: H-nanosheet (RDH15MR-H), ♦: annealed H-nanosheet (RDH15MR-H-400˚ C) and ♦: Degussa P25 as reference sample.

In the second series (figure 4.3), we examined annealed exchange nanowire and nanofiber (small nanowire produced by reflux method). We compared them with anatase microfiber produced from $K_2Ti_2O_5$ (synthesis already described somewhere in the manuscript ?) and P25. The nanowire is different from nanotube and nanosheet, it has bidentate carbonate intercalated in between the layers. Their presence causes it to transform to metastable TiO_2(B) phase between 400˚C to 800˚C. Therefore, we took both the 400˚C and 800˚C nanowire to compare. We discovered they also have worse adsorption ability than P25. The TiO_2(B) nanowire (RDH10M180-H-400˚ C) has a worse activity than other anatase ones, but it is still better active than nanotube. 800˚C annealed nanowire has similar efficency with

nanosheet mentioned above. The nanofiber has the best photoactivity. Although its adsorbability is less than P25, but the slope is shaper than P25. This implies it may have better efficiency than P25. Another point worth to discuss is nanofiber is more active than nanowire. They are both the same structure but nanofiber is much smaller. Even though the nanofiber has smaller specific surface than nanosheet, it still has better efficiency. As mentioned above in introduction, the less default (more crystallized) and more preferred orientation sample lead to a better efficiency. If they have the same structure, the smaller sample is better. These observations provide a route to improve and modify the photocatalytic activity of TiO_2 nanostructure.

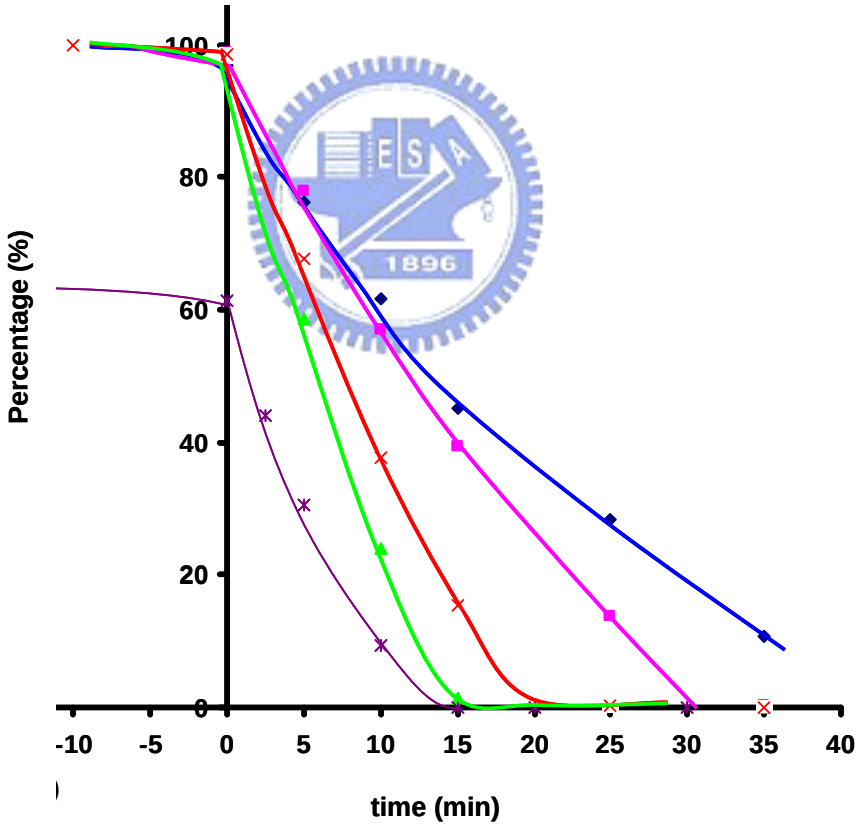

Figure 4.3. Photocatalytic activity of ♦: 400˚ C annealed H-nanowire (RDH10M180-H-400˚ C), ■: 800˚ C annealed H-nanowire (RDH10M180-H-800˚ C), ▲: 800˚ C annealed H-nanofiber (am15MR-H-800˚ C), x: 400˚ C annealed H-$K_2Ti_2O_5$ and *: Degussa P25 as reference sample.

4.3.2. Lithium ion intercalation property of titanate nanostructures

The lithium ion intercalated characteristics depend on the structure of TiO_2. TiO_2(B) has two peaks occurring at 1.5V and 1.6V in Cyclic voltammogram. The anatase peak is single and broad at 2.2V. Figure 5.4 and 5.5 are comparison of bulk TiO_2(B), annealed exchanged nanotube and nanofiber. We can observe the nanotube one presents typical feature of anatase with default which makes it having less capacity and reversibility. The nanofiber is much smaller than TiO_2(B) microfiber, therefore it has a bigger capacity (250mAh) than bulk one (140mAh).

The TiO_2(B) nanofiber (small nanoribbon) and microfiber have both a big unique peak (irreversible capacity) at 1.5V in the first cycle, but the nanotube one has not. We think that this peak is due to intercalated carbonate. In our above observations, the TiO_2(B) samples have carbonate but nanotube has not. The nanofiber is produced by reflux, so that it has more carbonate. We can obviously observe its first peak is stronger than the bulk one.

For comparison of nanoribbon (RDH10M180-H-400˚C), small nanoribbon (am10MR-H-400˚C) and longer nanoribbon (sodium carbonate additive nanoribbon, am10M180-0.8CO3-H-400˚C) (See figure 4.6 and 4.7), we can observe the small nanoribbon has more rapid intercalation speed. It is able to keep the resolution of CV curve even in higher charge rate (figure 4.6). The additive carbonate one has worse reversibility than others due to the carbonate which reacts with lithium or occupied the reversible active site. Moreover, the larger length leads to worse diffusion rate of lithium ion than other two samples.

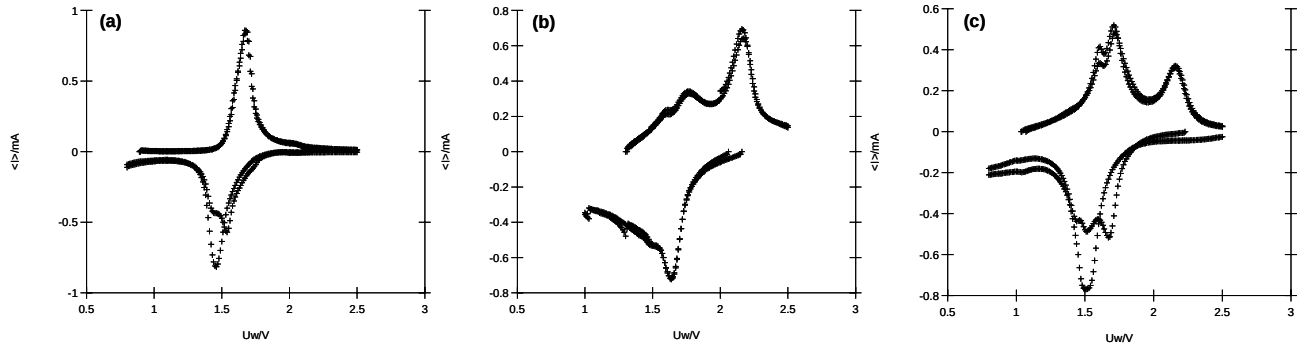

Figure 4.4. Cyclic voltammogram on the (a) bulk TiO_2(B) produced from $K_2Ti_4O_9$, (b) TiO_2 from nanotube (RDH140-H-400˚ C) and (c) nanofiber (am10MR-H-400˚ C) electrode (rate of charge: 2C).

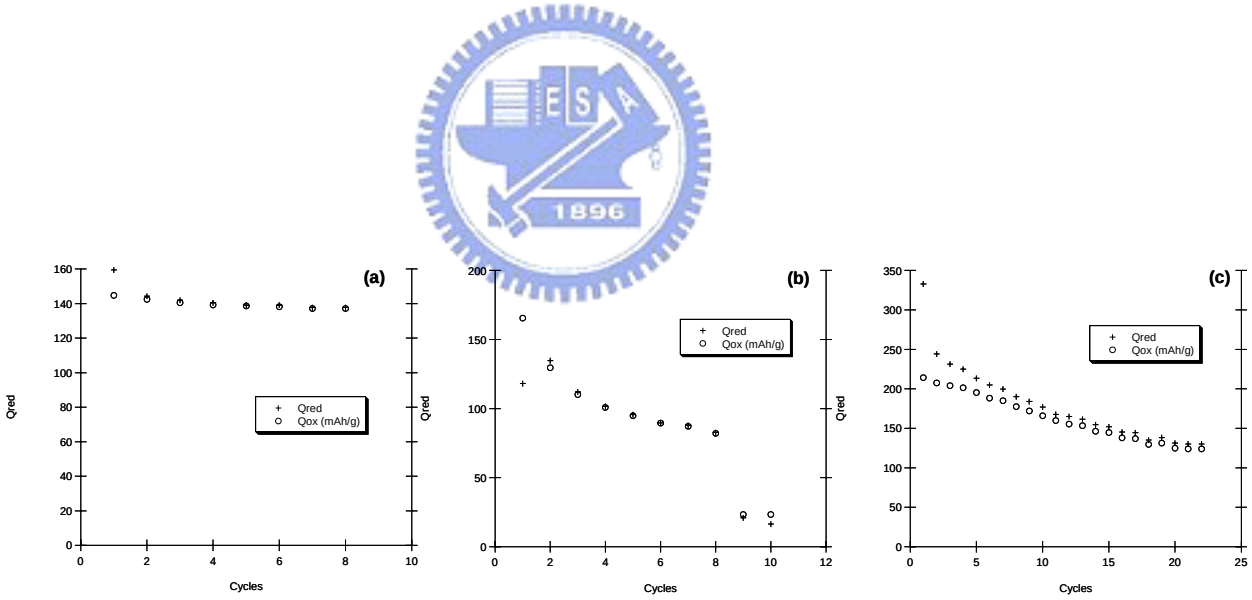

Figure 4.5. Charge-discharge curve on the (a) bulk TiO_2(B) produced from $K_2Ti_4O_9$, (b) TiO_2 from nanotube (RDH140-H-400˚ C) and (c) nanofiber (am10MR-H-400˚ C) electrode (rate of charge: 2C).

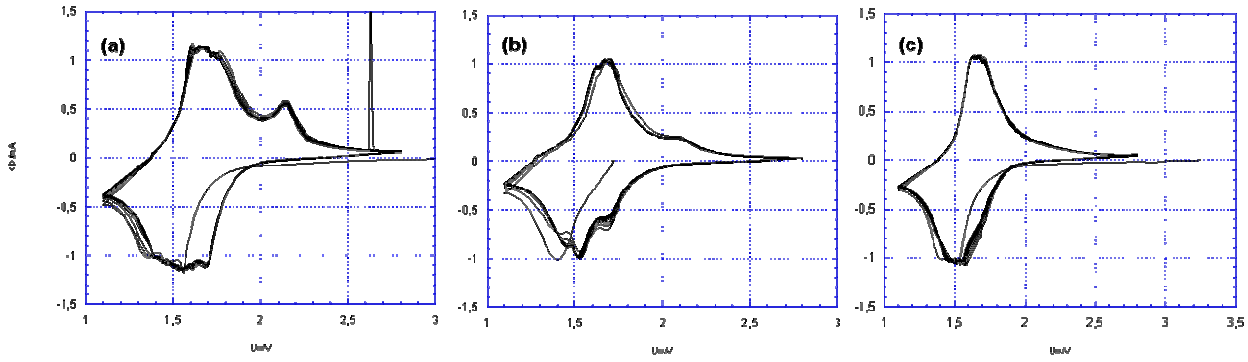

Figure 4.6. Cyclic voltammogram on the (a) nanoribbon (RDH10M180-H-400° C, reversible capacity: 140 $mAhg^{-1}$), (b) small nanoribbon (am10MR-H-400° C, reversible capacity: 140 $mAhg^{-1}$) and (c) longer nanoribbon (am10M180-0.8CO3-H-400° C, reversible capacity: 95 $mAhg^{-1}$) electrode (rate of charge: C).

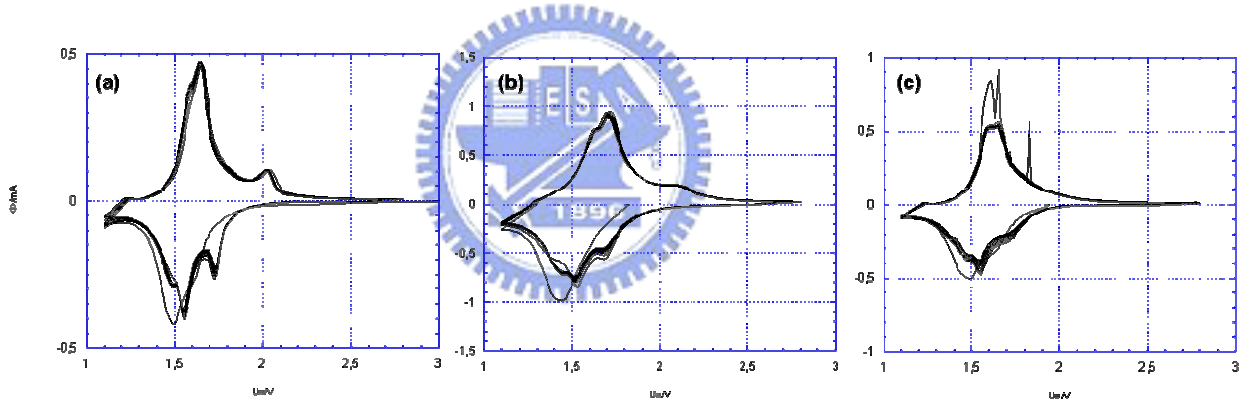

Figure 4.7. Cyclic voltammogram on the (a) nanoribbon (RDH10M180-H-400° C, reversible capacity: 170 $mAhg^{-1}$), (b) small nanoribbon (am10MR-H-400° C, reversible capacity: 165 $mAhg^{-1}$) and (c) longer nanoribbon (am10M180-0.8CO3-H-400° C, reversible capacity: 150 $mAhg^{-1}$) electrode (rate of charge: C/10).

4.4. Conclution

In the study of photocatalytic activity, we discovered the annealed exchanged nanoribbon, nanosheet and nanofiber (small nanoribbon) are photoactive. They all have similar even better efficiency than P25, but lower adsorbability of reactant due to the existence of absorbed carbonate. The nanoribbon and nanofiber have better photoactivity due to the more crystallized, even though their specific areas are smaller than the one of nanosheet. Therefore, the most important key to improve the efficiency is less stacking faults and more active site, the second is bigger specific surface.

In the study of lithium intercalation, we found the TiO_2(B) phase samples have better property. The structural carbonate causes an irreversible capacity in the beginning. As the rule mention above, the structure designs the property of material; the smaller crystal size has better efficiency when considering a same phase.

4.5. Reference

[1] O. Carp, C. L. Huisman and A. Reller, *Prog. Solid State Chem.* **2004**, *32*, 33–177.

[2] M. Zhang, Z. Jin, J. Zhang, X. Guo, J. Yang, W. Li, X. Wang and Z. Zhang, *J. of Molecular Catalysis A: Chemical* **2004**, *217*, 203–210.

[3] M. Hodos, E. Horváth, H. Haspel, Á. Kukovecz, Z. Kónya and I. Kiricsi, *Chem. Phys. Lett.* **2004**, *399*, 512–515

[4] H. Tokudome and M. Miyauchi, *Chem . Comm.* **2004**, 958–959.

[5] H. Tokudome and M. Miyauchi, *Chem. Lett.* **2004**, *33*, 1108-1109.

[6] X. Wang, Z. Jin, C. Feng, Z. Zhang and H. Dang, *J. Solid State Chem.* **2005**, *178*, 638–644.

[7] M. Wang, D. Guo and H. Li, *J. Solid State Chem.* **2005**, *178*, 1996–2000.

[8] S. H. Chien, Y. C. Liou and M. C. Kuo, *Synthetic Metals* **2005**, *152*, 333–336.

[9] V. Štengl , S. Bakardjieva, J. Šubrt, E. Večerníková, L. Szatmary, M. Klementová and V. Balek, *Applied Catalysis B: Environmental* **2006**, *63*, 20–30.

[10] S. Y. Huang, L. Kavan, I. Exnar, and M. Gratzel, *J. Electrochem. Soc.* **1995,** *142*, L142.

[11] Y. Zhou, L. Cao, F. Zhang, B. He, and H. Li, *J. Electrochem. Soc.* **2003**, *150*, A1246-A1249.

[12] M. Zukalová, M. Kalbáč, L. Kavan, , I. Exnar, and M. Graetzel, *Chem. Mater.* **2005,** *17,* 1248-1255.

[13] A. R. Armstrong, G. Armstrong, J. Canales, and P. G. Bruce, *Angew. Chem. Int. Ed.* **2004**, *43*, 2286 –2288.

[14] M. Karkmaz, E. Puzenat, C. Guillard, J.M. Herrmann, *Applied Catalysis B: Environmental* **2004**, *51*, 183–194.